Optical Materials 166 (2025) 117228

Contents lists available at ScienceDirect

Optical Materials

journal homepage: www.elsevier.com/locate/optmat

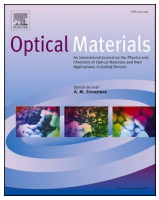

Research Article

Optical refractive properties and phonon spectra of Na_2SO_4 single crystal

M. Ya Rudysh [a], B.V. Andriyevsky [b,*], P.A. Shchepanskyi [a], M. Karkulovska [c], V. Yo Stadnyk [a], L. Bychto [b], R.S. Brezvin [a]

[a] Physics Faculty, Ivan Franko National University of Lviv, Kyrylo and Mefodii Str. 8, Lviv 79005, Ukraine
[b] Faculty of Electronics and Computer Sciences, Koszalin University of Technology, Śniadeckich Str. 2, PL-75-453, Koszalin, Poland
[c] Department of General Physics, Lviv Polytechnic National University, S. Bandery Str., 12, Lviv, 79013, Ukraine

ARTICLE INFO

Keywords:
Sodium sulfate
Refractive indices
Density functional theory
Infrared spectra
Phonons

ABSTRACT

Na_2SO_4 crystal was grown by slow evaporation method from an aqueous solution. Using the PXRD method, the crystal structure of Na_2SO_4 was investigated at room temperature, and it was found that the crystal belongs to the orthorhombic symmetry of the space group *Fddd* (no. 70) with the following unit cell parameters: $a = 5.8568(4)$ Å, $b = 12.2957(7)$ Å, $c = 9.809(1)$ Å, and $V = 706.52(8)$ Å^3. The dispersion of the refractive indices of Na_2SO_4 crystal in the visible and ultraviolet ranges was measured at room temperature and the principle refractive indices of optical indicatrix were determined to be $n_X = 1.4703$, $n_Y = 1.4847$, and $n_Z = 1.47669$ for the wavelength $\lambda = 500$ nm. The first-principle calculations of the phonon properties of the crystal were performed using the lattice dynamics method and DFPT approach. The polarized normal incidence reflection spectra of Na_2SO_4 crystal were measured in the infrared range 50–1300 cm^{-1} by using FTIR spectrometer and synchrotron radiation. The calculated reflection spectra of Na_2SO_4 crystal are in very good agreement with the experimental ones. In Na_2SO_4 crystal, the Reststrahlen band in the spectral range of 1120–1200 cm^{-1} is confirmed experimentally and theoretically.

1. Introduction

Sodium sulfate (Na_2SO_4) is a crystal with a wide range of applications, especially in research involving the detection of ionizing radiation. This compound is of particular interest for its potential applications in supercapacitors, enabling efficient energy storage and accumulation [1]. Additionally, the properties of these materials, especially when enhanced with nanoparticles, are being actively investigated [2]. Concurrently researched are the luminescent properties of pure and doped Na_2SO_4 crystals, along with their various composite formulations [3]. One of the key applications of the crystal is as a thermoluminescent dosimeter (TLD). TLDs have the ability to accumulate energy and release it as light when heated, which makes Na_2SO_4 a promising material for measuring ionizing radiation in various fields, such as medical diagnostics and radiation safety [3].

The recent study on a sodium sulfate/silica (Na_2SO_4/SiO_2) composite revealed that the material has a clear thermoluminescent glow peak between 150 °C and 200 °C. The glow curve remains stable across repeated irradiation cycles, showing good linearity with exposure. This makes Na_2SO_4 a reliable material for dosimetry applications [3].

Phase transitions in crystals play an important role in changing their physical and mechanical properties. These transitions can significantly change the structural parameters of crystals and their response to the external influences, such as pressure and temperature [4–7]. Na_2SO_4 crystals exhibit five distinct phase states. According to the literature, the compound undergoes the following sequence of phase transitions:

$$V \xrightarrow{473K} III \xrightarrow{503K} II \xrightarrow{510K} I \xrightarrow{1156K} \text{liquid}.$$

The symmetries of these phases are as follows: V – *Fddd* (D_{2h}^{24}, $Z = 8$); III – *Cmcm* (D_{2h}^{17}, $Z = 4$); II – *Pbnm* (or *Pnam*, D_{2h}^{16}, $Z = 4$); and I – $P6_3/mmc$. In the case of Na_2SO_4, phase transitions between different modifications of the crystal lattice have a significant effect on its thermoluminescent and elastic properties, which is important for its use as a dosimeter. The mechanical properties of Na_2SO_4, such as plasticity and elasticity, and their changes under pressures, may affect their thermoluminescent behavior, that is crucial for developing more efficient TLDs.

The impurities in Na_2SO_4 crystal can significantly affect its behavior

* Corresponding author.
E-mail addresses: rudysh.myron@gmail.com.bohdan (M.Y. Rudysh), bohdan.andriyevskyy@tu.koszalin.pl (B.V. Andriyevsky), pavloshchepanskyi@gmail.com (P.A. Shchepanskyi), mariana.s.karkulovska@lpnu.ua (M. Karkulovska), vasylstadnyk@ukr.net (V.Y. Stadnyk), leszek.bychto@tu.koszalin.pl (L. Bychto), brezvinr@ukr.net (R.S. Brezvin).

https://doi.org/10.1016/j.optmat.2025.117228
Received 15 April 2025; Received in revised form 6 June 2025; Accepted 7 June 2025
Available online 7 June 2025

as a TLD, improving its sensitivity and signal stability [8]. In addition to the thermoluminescent characteristics, the elastic properties of Na_2SO_4 are also important, which have a critical effect on the resistance of the material to mechanical deformations under high temperatures and pressures [9].

Na_2SO_4 crystals exhibit ionic conductivity, which in the V phase at room temperature demonstrates significant anisotropy [10,11]. The highest conductivity is observed along the [101] and [10 $\bar{1}$] directions, attributed to the presence of the open and interconnected channels that facilitate Na^+ ion diffusion. In contrast, the high-temperature phases exhibit isotropic conductivity in all directions [11].

Additionally, Na_2SO_4 crystals are promising materials for energy storage applications, particularly in thermal energy storage systems [12]. Understanding the optical and vibrational spectra of these crystalline materials is crucial for explaining their properties, as well as assessing their practical applications, potential, and limitations. Considering the thermoluminescent application of Na_2SO_4 crystals, the study of their optical properties in the wide spectral range, especially in the far-infrared spectral range, may be useful. This is because the temperature dependence of the specific heat capacity of a material, determining the effectiveness of the thermal energy exchange in it, depends on its phonon energy structure. To interpret the results of the optical measurements of a crystal in the far-infrared range precisely the knowledge of the corresponding high-frequency dielectric permittivity ε_∞ is crucial. That is why the precise measurements of the refractive indices of Na_2SO_4 crystals in the visible (VIS) and near-infrared range is also of interest.

2. Research methods

2.1. Crystal growth method

Na_2SO_4 crystals were obtained by slow evaporation of the saturated solution. Demineralized water was used as the solvent, where the starting salt dissolves well. Na_2SO_4 salt of 99.99 % purity was used for the crystal growth. Sodium sulfate salt was dissolved in the demineralized water according to the solubility table and stirred for 2 h using a magnetic stirrer. After completely dissolving the salt in water, the resulting solution was filtered with filter paper. The crystal growth occurred in a crystallization dish during slow evaporation of the solvent at a constant temperature. Multiple recrystallization of the salt with repeated filtration of the solution was used to obtain high-quality pure single crystals. Single crystal growth occurred from seeds spontaneously formed at the bottom of the crystallization dish. The crystal growth process took 30–50 days, resulting in crystals of size $9 \times 8 \times 15$ mm^3.

2.2. Crystal structure study

The structure of the grown crystals was studied using the powder X-ray diffraction technique. The sample under study was in the form of a powder, to obtain which the single-crystal sample was ground in an agate mortar. It was applied in a uniform layer on a polymer film and fixed with another film. Experimental intensities and reflection angles of the sample were obtained using an automatic diffractometer STOE STADI P (manufacturer STOE & Cie GmbH, Germany) with a linear position-precise detector (PSD) [13] according to a modified Guinier geometry scheme. The main parameters were: Cu Kα1 radiation source; detector – concave Ge monochromator (111) of the Johann type; scanning – 2θ/ω; interval of angles 2θ - 2.500° ≤ 2θ ≤ 100.405°, with a step of 0.015°; detector step 0.480°; voltage $U = 40$ kV; current $I = 37$ mA. The experimental diffractograms were processed using the STOE WinXPOW [13] and PowderCell [14].

2.3. Study of refractive parameters

The wavelength dependence of the refractive indices $n(\lambda)$ was studied by the standard Obreimov immersion method [15,16]. For this purpose, a special Obreimov attachment with a crystal holder, a cuvette, and an eyepiece was used. The method is based on comparing the refractive indices of a crystalline sample and a known liquid (immersion liquid) using light polarized along the selected direction of the sample. A mixture of α-monobromonaphthalene and refined petroleum was used as the immersion liquid, which met the criteria for such liquids [17]. The method provides an accuracy of measurement of refractive indices of 2×10^{-4} and allows obtaining a refractive index value in the range of 1.45–1.65 in the wavelength range of approximately 400–750 nm. The refractive indices n_i of the crystal were measured for the principal axes $i = X, Y,$ and Z of the optical Fresnel ellipsoid, which are parallel to the crystallographic axes b, c, and a, respectively. For this purpose, samples were cut from the grown crystal in the form of thin oriented plates. They were cut in the XY and XZ planes, which allowed the refractive indices to be measured in three crystallographic directions. The plates were oriented according to the appearance of conoscopic patterns and the extinction of the crystal in a polarizing microscope. The cut plates were polished using diamond pastes of different grain sizes.

2.4. Measurements of the reflection spectra of Na_2SO_4 crystal in the infrared range

Measurements of the specular reflectance of Na_2SO_4 crystal were performed in the IR spectral range 60–1300 cm^{-1} at near normal radiation incidence (angle of incidence was equal to 9°) using the synchrotron radiation of BESSY II storage ring at the IRIS beamline of HZB (Berlin) [18]. The reflection spectra of the polished crystal were measured for two mutually perpendicular positions corresponding to the radiation polarization along the acute and obtuse bisectors of the angle between optical axes of Na_2SO_4 crystal.

2.5. Calculation of the phonon spectrum

Calculations of the phonon spectrum of the Na_2SO_4 crystal were carried out using the CASTEP program [19] within the framework of the density functional perturbation theory (DFPT) [20–22]. The initial information for the calculations was the crystallographic data obtained for the synthesized crystal in this work. To describe the exchange-correlation functional, the generalized gradient approximation GGA [23] with the Perdue-Burke-Ernzerhoff (PBE) parameterization [24] was used. The electron-nuclear interaction was described using the ultrasoft Vanderbilt pseudopotential [25] and the norm-conserving one [26]. The following electronic configuration was used in the calculations: Na $2s^2\ 2p^6\ 3s1$; S $3s^2\ 3p^4$; O $2s^2\ 2p^4$. The basis was chosen in the form of plane waves. The maximum kinetic energy of plane waves was $E_{\text{cut-off}} = 750$ eV. The integration was performed over the k-mesh $6 \times 3 \times 3$ of the first Brillouin zone. Before calculating the phonon spectrum of the crystal, geometric optimization of the crystal lattice was carried out using the BFGS method [27]. During this procedure, the following convergence criteria were used: the self-consistent field convergence $E = 5.0 \times 10^{-7}$ eV/atom; the total energy convergence $E = 5.0 \times 10^{-6}$ eV/atom; the maximum force 0.01 eV/Å; the maximum stress 0.02 GPa; the maximum displacement 5.0×10^{-4} Å.

3. Results and discussion

3.1. Structure of Na_2SO_4 crystals

The Na_2SO_4 single crystals obtained by evaporation were homogeneous, transparent, colorless, and had good optical quality. Their optical quality was checked by the appearance of conoscopic patterns and by extinction under a polarizing microscope. The inset of Fig. 1 shows a

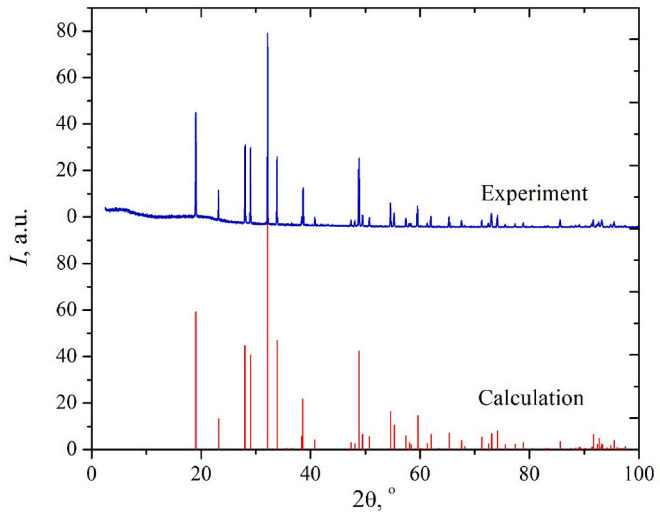

Fig. 1. Diffraction patterns obtained experimentally for powder samples of Na_2SO_4 crystal (top of the figure) and calculated on the basis of the optimized Na_2SO_4 crystal structure (bottom of the figure).

photograph of a grown Na_2SO_4 crystal. The crystals had a shape close to a quadrangular prism. The crystal structure is layered with layers perpendicular to the longer axis of the prism. During crystal orientation, it was found that the optical axes are located in the plane of the crystal layers. The same arrangement of the optical axes was previously obtained for a $LiNH_4SO_4$ crystal grown in the α-modification [28], where the optical axes are located in the plane of the layers parallel to the single crystal grown in the form of a plate.

X-ray diffraction from powder samples verified the grown crystal's structure. Fig. 1 shows the diffractogram obtained for the Na_2SO_4 crystal. Here, the blue line corresponds to the experimental diffractogram, and the purple line corresponds to the theoretical one. The synthesized single crystal turned out to be single-phase. The Na_2SO_4 compound (room temperature modification) has orthorhombic symmetry with the *Fddd* space group symmetry (no. 70) and its own structural type. The refined unit cell parameters are as follows: $a = 5.8568(4)$ Å, $b = 12.2957(7)$ Å, $c = 9.809(1)$ Å, volume $V = 706.52(8)$ Å^3. For comparison of the obtained structural data, Table 1 presents other experimental crystallographic data from Ref. [29]. Table 2 contains the experimental atomic coordinates. The crystallographic data obtained are in good agreement with the data available in the literature and confirm the phase of the grown crystal. The tables show that the theoretical lattice parameters and cell volume are overestimated compared to the experimental ones. This behavior is typical for the use of the GGA functional in the DFT framework.

The structure of the Na_2SO_4 crystal lattice constructed from the experimental data obtained in this work is shown in Fig. 2. The main structural units in the crystal are the tetrahedral anionic complexes SO_4^{2-}, which are likely to be predominantly responsible for the properties of the crystal. The sodium ions are located in the cavities formed by the anion tetrahedra.

Table 1
Experimental [29] and calculated using the GGA functional, the crystallographic parameters of the Na_2SO_4 crystal.

Parameter	Ref. [29]	Experiment	GGA
a, Å	5.85	5.8568(4)	5.9551
b, Å	12.29	12.2957(7)	12.4898
c, Å	9.75	9.809(1)	9.9949
V, Å^3	701	706.520(8)	743.418

Table 2
Experimental (this work) and calculated using the GGA functional, the fractional coordinates of atoms in the Na_2SO_4 crystal.

Atom	Exp.			GGA		
	x/a	y/b	z/c	x/a	y/b	z/c
Na	1/8	1/8	0.4406(3)	1/8	1/8	0.4517
S	1/8	1/8	1/8	1/8	1/8	1/8
O	0.2681(4)	0.0537(2)	0.0396(3)	0.2876	0.0557	0.0401

3.2. Refractive parameters of the Na_2SO_4 crystal

Information about the dispersion of the refractive indices $n_i(\lambda)$, where $i = X, Y, Z$, makes it possible to estimate the refractive characteristics of the material, which are closely related to its electronic subsystem. Since the Na_2SO_4 crystal belongs to the orthorhombic symmetry, its optical properties are determined by the dielectric function tensor, which contains three independent components ε_{11}, ε_{22}, and ε_{33}. For the measurement, samples in the form of thin plates cut in planes perpendicular to the crystal-physical directions were used. The plates were 0.1–0.5 mm thick and had plane-parallel faces with well-polished surfaces. It was established that the Na_2SO_4 crystal is an optically biaxial one with three independent refractive indices, $n_X \neq n_Y \neq n_Z$. The dispersion of refractive indices was studied in the wavelength range of 400–750 nm.

Fig. 3 shows the dispersion of refractive indices of Na_2SO_4 crystal for three crystal-physical directions. Here, the notation used is that the directions *X*, *Y*, and *Z* correspond to the direction of the acute bisector of the angle between optical axes, the obtuse bisector of the angle between optical axes, and the perpendicular to the plane of the optical axes, respectively. The crystal-physical directions *X*, *Y*, and *Z* of Na_2SO_4 are parallel to the following principal axes of optical indicatrix, $X \,||\, N_p$, $Y \,||\, N_g$, and $Z \,||\, N_m$. It can be seen from the figure that in the studied spectral range, the refractive indices undergo a smooth change, which indicates the absence of absorption bands in this spectral region. Thus, the fundamental optical absorption edge caused by the electron excitations of the crystal is in the ultraviolet (UV) region, and the crystal is transparent in the range of 400–750 nm. This behavior is inherent in the entire studied spectral range. It is worth noting that similar wavelength dependences of the refractive indices $n(\lambda)$ were previously observed for $LiNaSO_4$ [31] and $NaNH_4SO_4$ [32] crystals. The dispersion of the refractive index is normal ($dn/d\lambda < 0$), and the dispersion changes for the wavelength $\lambda = 500$ nm are as follows: $dn_x/d\lambda = -5.58 \times 10^{-5}$ nm^{-1}; $dn_y/d\lambda = -4.54 \times 10^{-5}$ nm^{-1}; $dn_z/d\lambda = -4.99 \times 10^{-5}$ nm^{-1}. It was found that the Na_2SO_4 crystal is optically positive in the spectral range studied (Fig. 3 and Table 3). However, the crystal may become optically negative in the spectral range $\lambda > 750$ nm.

The average refractive index of the Na_2SO_4 crystal is 1.4772 and is greater than the average refractive index of the $NaNH_4SO_4 \times 2H_2O$ crystal (1.4536). The increase in the refractive index can be attributed to the higher density of Na_2SO_4 crystal, which is equal to $\rho = 2.675$ g/cm^3 compared to $\rho = 1.745$ g/cm^3 of $NaNH_4SO_4 \times 2H_2O$. At the same time, the average refractive index is smaller than the value obtained for the optically uniaxial $LiNaSO_4$ crystal (1.49613) [31].

The Sellmeier formula is often used to describe the dispersion of refractive indices $n(\lambda)$ of dielectric crystals [16],

$$n_i^2 = 1 + \frac{B_1\lambda_{01}^2\lambda^2}{\lambda^2 - \lambda_{01}^2} + \frac{B_2\lambda_{02}^2\lambda^2}{\lambda^2 - \lambda_{02}^2}, \quad (1)$$

where λ_{01} and λ_{02} are the wavelengths of the effective centers of the UV and infrared (IR) absorption bands, and B_1 and B_2 are quantities related to the effective strengths of the UV and IR oscillators. In practice, for materials transparent in the VIS and near-IR ranges, for which the relation $\lambda_{02} \gg \lambda$ is valid, the following simplified Sellmeier formula is used for the wavelength dependence of the refractive index $n(\lambda)$ in these

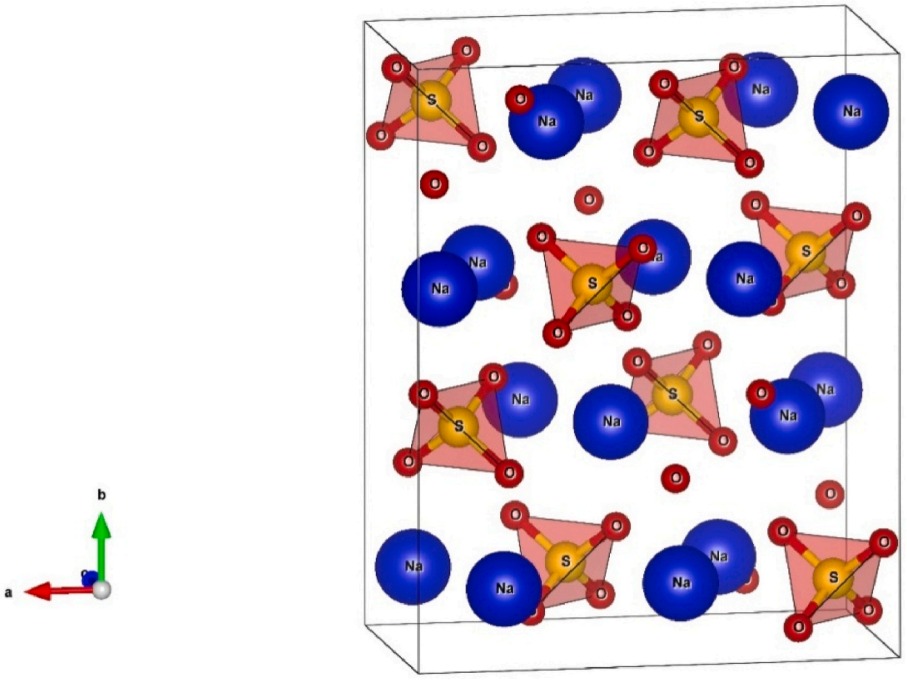

Fig. 2. Structure of the unit cell of Na_2SO_4 crystal drawn using the VESTA program [30].

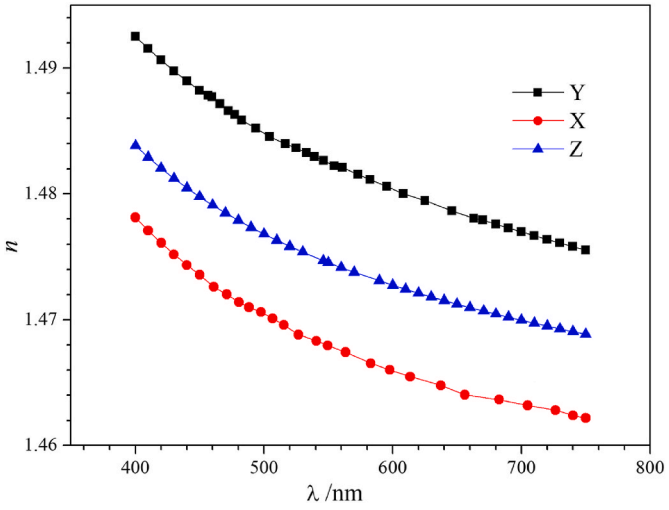

Fig. 3. Dispersion of refractive indices of Na_2SO_4 crystal at room temperature.

Table 3
Experimental refractive indices of some crystals of the A_2BX_4 group for the wavelength of λ = 500 nm.

Crystal	n_X	n_Y	n_Z
Na_2SO_4	1.4703	1.4847	1.4767
$NaNH_4SO_4 \times 2H_2O$ [31]	1.4602	1.4576	1.4430
$LiNaSO_4$ [30]	1.4939	1.4939	1.5006

spectral ranges,

$$n_i^2 = 1 + \frac{B_1\lambda_{01}^2\lambda^2}{\lambda^2 - \lambda_{01}^2} - B_2\lambda^2 . \quad (2)$$

Using the relation (2), the dispersion curves corresponding to three crystal-physical directions of Na_2SO_4 crystal were fitted. As a result of the approximation, the positions of the effective centers of the UV and infrared absorption bands and the quantities related to the effective forces of the corresponding oscillators were obtained. The values of the obtained parameters are collected in Table 4.

The orthorhombic symmetry of Na_2SO_4 crystal leads to the anisotropy of its optical indicatrix. A knowledge of the parameters of the optical indicatrix of crystal may be used in various optical-and-polarization applications. To estimate the degree of Na_2SO_4 optical indicatrix, we have used the anisotropy coefficient A_{n-1} in the following form,

$$A_{n-1} = \sum_{\substack{ij=1 \\ i\neq j}}^{3} \frac{|(n_i - 1) - (n_j - 1)|}{(n_i - 1) + (n_j - 1)}, \quad (3)$$

where $i = 2 \rightarrow 3 \rightarrow 1$ and $j = 1 \rightarrow 2 \rightarrow 3$ and n_1, n_2, n_3 are the principal refractive indices. The spectral dependence of this coefficient $A_{n-1}(\lambda)$ was found to be of the maximum-like form (Fig. 4), indicating a smaller anisotropy in the UV and near-IR ranges compared to the wavelength λ = 510 nm. Besides, a value of the anisotropy coefficient A_{n-1} represents the degree of anisotropy of the electron subsystem of the crystal. It is worth to mention that the substitution of the cation K → Na in the corresponding sulfates leads to the increase in the refractive index anisotropy coefficient from 0.008 (at λ = 500 nm) for K_2SO_4 [33] to 0.0307 for Na_2SO_4 (at λ = 520 nm), which indicates the increase of 26 %.

Experimental values of refractive indices are related to the electronic polarizability and refractivity of the material. The relationship between these quantities is described by the Lorentz–Lorenz formula [17],

Table 4
The parameters of the Sellmeier formula of the Na_2SO_4 crystal obtained for room temperature.

Axis	λ_{01}, nm	B_1, $\times 10^{-4}$ nm^{-2}	B_2, $\times 10^{-8}$ nm^{-2}
X	90.1	1.385	0.782
Y	83.5	1.690	2.870
Z	83.4	1.654	1.561

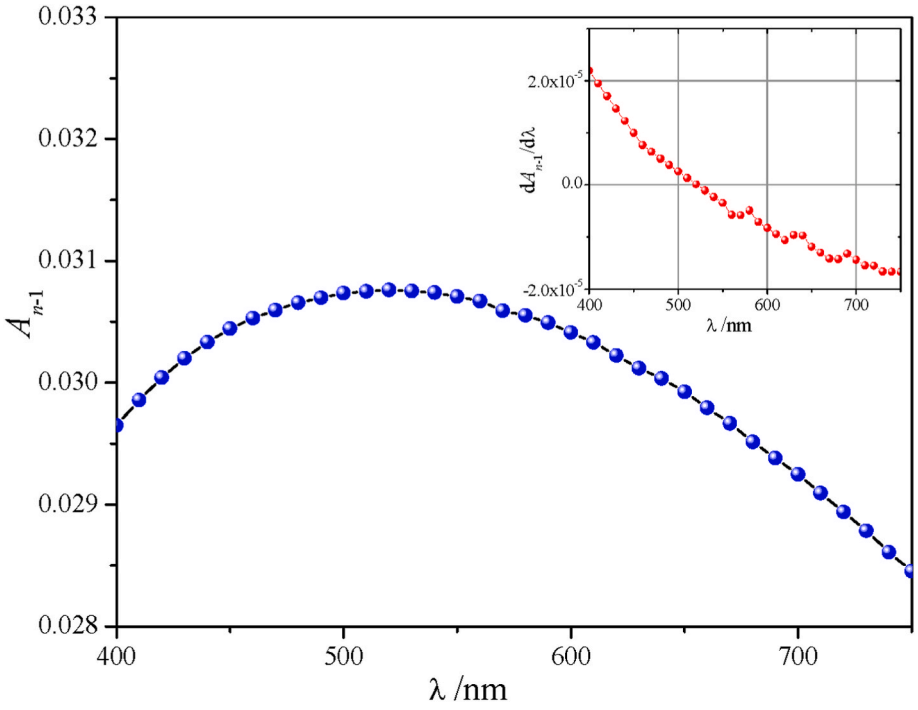

Fig. 4. Spectral dependence of the refractive index anisotropy coefficient A_{n-1} for Na_2SO_4 crystal. Wavelength dependence of the derivative $dA_{n-1}/d\lambda$ is presented in the inset.

$$R_i = \frac{n_i^2 - 1}{n_i^2 + 2}\frac{M}{\rho} = \frac{4\pi\alpha_i N_0}{3}, \quad (4)$$

where n is the refractive index of the crystal, α is the electronic polarizability, R is the molar refractivity, ρ is the density of the crystal, M is the molar mass of the crystal, and N_0 is the atomic density. The obtained refractive parameters are collected in Table 5.

According to the additive principle applied to refractivity [34], the calculated sum of the molar refractivity of individual structural elements of Na_2SO_4 is equal to

$$2R_{Na^+} + R_{SO_4^{2-}} \approx 2 \times 0.7 + 14.5 = 15.9\ \text{cm}^3, \quad (5)$$

which is slightly smaller than the calculated one for the wavelength λ = 500 nm (Table 5). The positive difference between the experimental and additive refractivities of Na_2SO_4 indicates the additional transfer of the outer electrons from Na^+ to SO_4^{2-} neighboring ions during the crystal growth of Na_2SO_4, which increases the polarizability and refractivity of the material as a whole. From the contributions of individual components to the total refractivity, it is clear that sodium ions have a much smaller effect on the total refractivity of the material, which is 8.8 % of the total refractivity of the Na_2SO_4 crystal. Previously, the refractivities $R_{X,Y} = 14.512\ \text{cm}^3/\text{mol}$ and $R_Z = 14.668\ \text{cm}^3/\text{mol}$ (for the wavelength λ = 500 nm) were obtained for $LiNaSO_4$ crystal [31], and the values $R_X = 27.183\ \text{cm}^3/\text{mol}$, $R_Y = 27.051\ \text{cm}^3/\text{mol}$, and $R_Z = 26.302\ \text{cm}^3/\text{mol}$ for $NaNH_4SO_4$ one [32]. Comparing these data, one can conclude that the cationic substitutions $Li^+ \rightarrow Na^+ \rightarrow NH_4$ lead to the increase in refractivity of the crystals mentioned, that is caused by the corresponding increase of the ionic refractivities, $R^+_{Li} = 0.2\ \text{cm}^3/\text{mol}$, $R^+_{Na} = 0.7\ \text{cm}^3/\text{mol}$, and $R^+_{NH4} = 11.96\ \text{cm}^3/\text{mol}$.

Table 5
Calculated from the relation (4) the molar refractivities R_i (i = X, Y, Z) and polarizabilities α_i of Na_2SO_4 crystal for the wavelength λ = 500 nm.

Crystall-physical axis	R_i, cm^3/mol	α_i, $10^{-24}\ \text{cm}^3$
X	21.49	8.52
Y	22.06	8.74
Z	21.75	8.62

3.3. Phonon spectra of Na_2SO_4 crystal

3.3.1. Theoretical phonon spectra of Na_2SO_4 crystal

Theoretical calculations of the vibrational spectrum of the Na_2SO_4 crystal were carried out within the framework of the density functional perturbation theory (DFPT) [21–23,35,36] using the GGA functional [24]. The lattice of the Na_2SO_4 crystal belongs to the space group of symmetry *Fddd* (no. 70) and contains 56 atoms in its structure (see Tables 1 and 2). Since the Na_2SO_4 crystal possesses a primitive lattice, only fourteen atoms (N = 14) in the primitive unit cell were used for the phonon calculations. Thus, the total number of the normal modes in the primitive unit cell of Na_2SO_4 is equal to 3 N = 42 (3 acoustic and 39 optical modes).

Fig. 5 shows the calculated phonon dispersion of the Na_2SO_4 crystal plotted in the direction Z → Γ → X → Y → Γ of the first Brillouin zone (a) and the phonon density of states (b). The vibrational spectrum consists of a set of vibrations, the frequencies of which range from 0 to 1149 cm^{-1}. In general, the vibrational spectrum is formed by the vibrational bands localized in several frequency ranges. This feature was obtained earlier for $LiNH_4SO_4$ crystals [37] and can be explained by the presence of weakly interacting complexes with strong internal coupling. The low-frequency region is formed by three acoustic branches LA, TA_1, and TA_2, the frequencies for which are the lowest. An absence of the negative frequencies in the phonon mode dispersions (Fig. 5(a)) indicates that the crystal under study is dynamically stable [38–41]. The upper limit of the frequency of acoustic modes is equal approximately 100 cm^{-1}. The low-frequency band covers vibrations in the range of 0–283 cm^{-1}. The next two vibration bands with weak dispersion are located near 450 cm^{-1} and 600 cm^{-1} of the phonon frequency. A narrow high-frequency band is observed at the frequency of 938 cm^{-1}. The highest vibrational band in the phonon spectrum is located in the frequency range of 1042–1149 cm^{-1}.

For a more detailed analysis of the vibrational spectrum of Na_2SO_4 crystal, the phonon partial density of states was calculated (Fig. 6). The

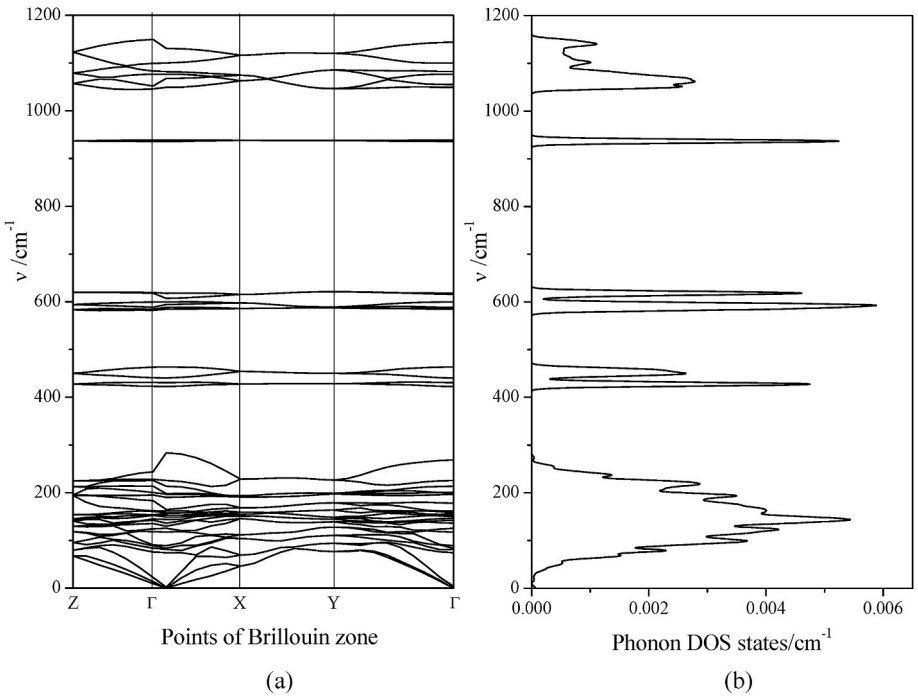

Fig. 5. Phonon mode dispersions (a) and total phonon density of states (b) of Na_2SO_4 crystal calculated using GGA functional and ultrasoft pseudopotentials.

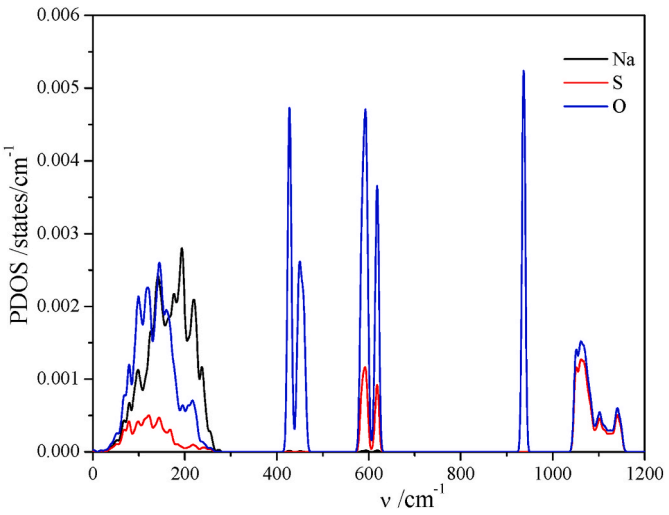

Fig. 6. Partial density of phonon states of the Na_2SO_4 crystal.

phonon states in the low-frequency range of 0–283 cm^{-1} are formed by all constituent atoms (sodium, sulfur and oxygen). The largest partial density of states in this range is from sodium and oxygen atoms, when the corresponding contribution from sulfur is here smallest.

In the groups 2 and 4, corresponding to the symmetric modes, the sulfur ion in the SO_4^{2-} tetrahedral anion of Na_2SO_4 crystal remains fixed during vibrations. The latter feature causes the absence of the partial density of phonon states for sulfur (Fig. 6).

The ideal isolated sulfate anion belongs to the T_d point group of symmetry, and its vibrational representation is: $\Gamma_v = A_1(\nu_1) + E(\nu_2) + F_2(\nu_3) + F_2(\nu_4)$. Only two triply-degenerated (F_2) modes, ν_3 (asymmetric stretching) and ν_4 (asymmetric bending), should be active in the IR spectrum [42].

Real symmetry of the sulfate anion is lower in Na_2SO_4 due to lower site symmetry than T_d (in fact D_2). It leads to the removal of the degeneracy and splitting of the ν_4 band to a doublet (for D_2 site symmetry, a triplet is expected) and the ν_3 band to an asymmetric triplet (consistent with D_2 site symmetry).

Fig. 7 contains the intensity of calculated infrared absorption of the Na_2SO_4 crystal observed in the infrared spectral range. According to symmetry considerations, among the 42 vibrational modes in the Na_2SO_4 crystal, 17 modes should be active in the infrared spectrum. The isolated SO_4^{2-} anion, possessing the T_d symmetry, has four types of vibrations: asymmetric (groups 1 and 3 of modes in Table 6) and symmetric (groups 2 and 4 of modes in Table 6). For the SO_4 anion, the groups of modes 1 and 3 are active in the infrared spectrum. The infrared spectrum bands near the frequency of 600 cm^{-1} correspond to the asymmetric O–S–O bending vibration mode of the group 3. The high-frequency vibrations in the spectral range 1042–1149 cm^{-1} correspond to the S–O asymmetric stretching vibration mode of the group 1 (Table 6). The obtained bands are in good agreement with the spectral position of the levels for the $LiNH_4SO_4$ crystal [37], for which the

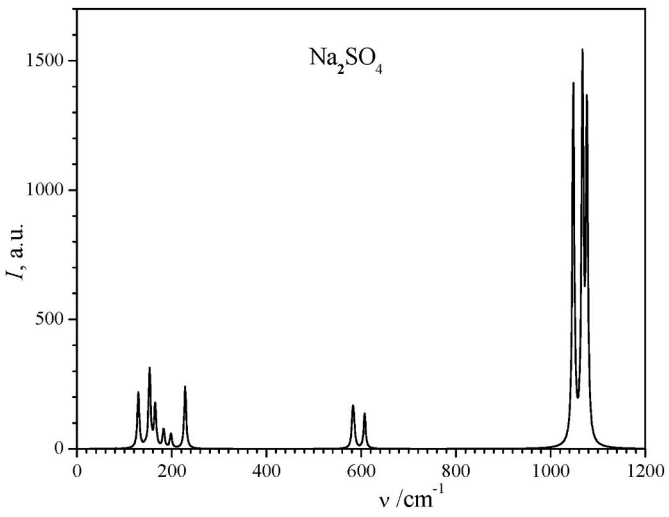

Fig. 7. Infrared spectra of Na_2SO_4 crystal calculated with the GGA-PBE functional using the ultrasoft pseudopotentials.

Table 6
Assignments of frequencies of partial density of phonon states of Na_2SO_4 crystal.

Group of modes	Frequency range of partial density of phonon states/cm^{-1}	Ion, vibration mode
1	1040–1150	SO_4^{2-}, asymmetric stretching
2	940	SO_4^{2-}, symmetric stretching
3	580–620	SO_4^{2-}, asymmetric bending
4	420–470	SO_4^{2-}, symmetric bending
5	40–260	Na_2SO_4

frequency of mode 1 coincides with that obtained for the Na_2SO_4 crystal, and the frequency of mode 3 is slightly shifted to the higher frequency region. The low-frequency maxima of infrared absorption in the range of 100–250 cm^{-1} correspond to the optical vibrational modes responsible for the mutual oscillation of Na cations and SO_4 anions in Na_2SO_4 crystal.

The sequence of the calculated components of the dielectric permittivity, $\varepsilon_{\infty X} < \varepsilon_{\infty Z} < \varepsilon_{\infty Y}$, of Na_2SO_4 (Table 7) is the same as the experimental refractive indices, $n_X < n_Z < n_Y$ (Table 3). The values of the calculated permittivities $\varepsilon_{\infty i}$ ($i = X, Y, Z$) are 4 % larger than the corresponding squares of experimental refractive indices n^2 (Table 3). This is caused by the known feature of the DFT calculations that resulted in the decrease of the crystal's band gap E_g and corresponding increase of the dielectric permittivity ε_∞.

The static dielectric permittivity ε_0 of Na_2SO_4 crystal (Table 7) were calculated by the CASTEP code as the response property with respect to an electric field perturbation of an insulating system [43]. The observed smallest dielectric permittivity ε_{0Z} in relation to the dielectric permittivities ε_{0x} and ε_{0y} (Table 7) is probably connected with the corresponding anisotropy of interatomic distances in Na_2SO_4: the lengths of Na - O interatomic bonds in Z-direction ($d^{(Z)}_{Na\text{-}O} = 0.253$ nm) are larger than the similar ones in X- and Y-directions ($d^{(X)}_{Na\text{-}O} = d^{(Y)}_{Na\text{-}O} = 0.233$ nm).

3.3.2. *Experimental spectra of Na_2SO_4 crystal in the infrared range*

In the whole IR spectral range studied, 50 - 1300 cm^{-1}, the reflection coefficient R of Na_2SO_4 crystal for the radiation polarized along the acute bisector of the angle between optical axes is larger than that for radiation polarized along the obtuse corresponding bisector (Fig. 8). The relation obtained for the reflection coefficients, $R^{(acute)} > R^{(obtuse)}$ (Fig. 8), is similar to that for the experimental refractive indices, $n_Y > n_X$ (Table 3), and theoretical dielectric permittivities, $\varepsilon_{\infty Y} > \varepsilon_{\infty X}$ and $\varepsilon_{0Y} > \varepsilon_{0X}$ (Table 7). Here, the directions y and x correspond to the maximum and minimum refractive indices (Table 3) and dielectric permittivities (Table 7). These similarities are resulted from the known relation, $R = (n - 1)^2/(n + 1)^2 = (\varepsilon^{1/2} - 1)^2/(\varepsilon^{1/2} + 1)^2$.

The spectral band in the range of 1120–1200 cm^{-1} is caused by the stretching vibrations of S – O bonds in SO_4^{2-} anion, when two maxima in the range of 610–650 cm^{-1} relate to the bending vibrations of O – S – O bonds in this group (Fig. 8). Similar structure is observed in the reflection spectrum of Rb_2SO_4 crystal [44]. The low-frequency peaks of the reflection spectrum $R(\nu)$ of Na_2SO_4 in the range $\nu < 260$ cm^{-1} are formed

Table 7
Dielectric permittivities ε_0 and ε_∞ of Na_2SO_4 crystal for the space group of symmetry *Fddd* (no. 70) calculated using CASTEP code with PBEsol exchange-and-correlation functional and norm-conserving pseudopotentials. The squares of experimental refractive indices $n^2 \approx \varepsilon_\infty$ (see Table 3) are shown in parenthesis (see Table 3).

Cartesian direction Permittivity	*X*	*Y*	*Z*
ε_∞	2.26219 (2.1618)	2.30251 (2.2043)	2.28705 (2.1806)
ε_0	6.00999	6.91158	4.40785

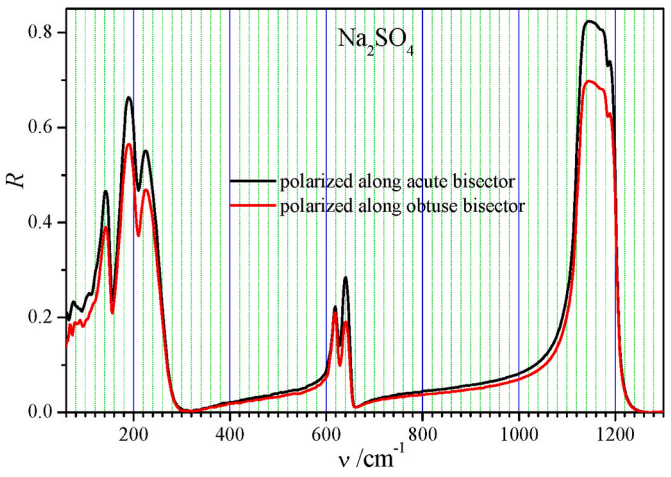

Fig. 8. Polarized reflection spectra of Na_2SO_4 crystal in the infrared range for two mutually perpendicular orientations of the sample.

by the collective vibrations of the sodium cations and SO_4^{2-} anion (Fig. 8), that is seen from the partial density of phonon states (Fig. 6).

The experimental reflection spectrum $R(\nu)$ for the radiation polarization along the acute/obtuse bisector of the angle between optical axes (Fig. 8) was fitted by the Kramers-Kronig relation using the RefFIT program [45] and the corresponding fitted reflection spectrum $R_{fit}(\nu)$ (Fig. 9(a)) and the dielectric function $\varepsilon(\nu) = \varepsilon_1(\nu) + i{\cdot}\varepsilon_2(\nu)$ (Fig. 9(b)) were obtained. The Drude-Lorentz model for the dielectric function $\varepsilon(\nu)$ was used for fitting the experimental reflectance spectra [45,46],

$$\varepsilon(\nu) = \varepsilon_\infty + \sum_{i=0}^{N} \frac{\nu_{pi}^2}{\nu_{0i}^2 - \nu^2 - i\gamma_i\nu} \,. \tag{6}$$

Here, ε_∞ is the 'high-frequency dielectric permittivity', which represents contribution from the electron oscillators of the bonded electrons to the total dielectric function $\varepsilon(\nu)$ of a material. The parameters ν_{pi}, ν_{0i} and γ_i are the 'plasma' frequency, the eigen-frequency and the damping rate, respectively, for the Drude free electrons term ($i = 0$) and Lorentz phonon oscillators ($i = 1,2, \ldots,N$). For the Drude free electrons term, the corresponding eigen-frequency, ν_{00} is equal to zero [46]. The fitting parameters obtained for Na_2SO_4 crystal are presented in Table 8.

Good quality of such fitting is confirmed by the values of the real part of dielectric permittivity at the frequency $\nu = 0$, $\varepsilon_1(0) = 6.1422$ (Fig. 9 (b)), which differs not very much from the DFT calculated one, $\varepsilon_{1Y} = 6.9116$ (Table 7). Once again, the latter relation, $\varepsilon_{1Y} > \varepsilon_1(0)$, is probably caused by known drawback of DFT calculations mentioned at the end of subchapter 3.2.1.

The relatively wide spectral band of the large reflection coefficient R in the range of 1120–1200 cm^{-1} (Fig. 8) indicates the Reststrahlen band [47]. This Reststrahlen band in Na_2SO_4 was pointed out in Ref. [48]. If the boundary frequencies 1120 cm^{-1} and 1200 cm^{-1} of this reflection spectral band are taken as the frequencies of the transversal and longitudinal optical phonons ν_{TO} and ν_{LO}, then the calculated values of the real part of dielectric permittivity $\varepsilon_s^{(local)}$ and ε_∞, shown in Fig. 9(b), satisfy the Lyddane-Sachs-Teller relation,

$$\frac{\nu_{LO}}{\nu_{TO}} = \sqrt{\frac{\varepsilon_s^{(local)}}{\varepsilon_\infty}} \,. \tag{7}$$

In the spectral range 1120–1200 cm^{-1} of stretching vibrations of S - O bonds, the real part of the dielectric function is negative (Fig. 9(b)), that corresponds to the observed Reststrahlen band, which is realized due to the relatively high ionicity character (IC) between S and O atoms [49],

$$IC = 1 - \exp[-0.25(X_S - X_O)^2] = 0.78, \tag{8}$$

where $X_S = 2.5$ and $X_O = 3.5$ are the electronegativities for the sulfur and oxygen atoms [46].

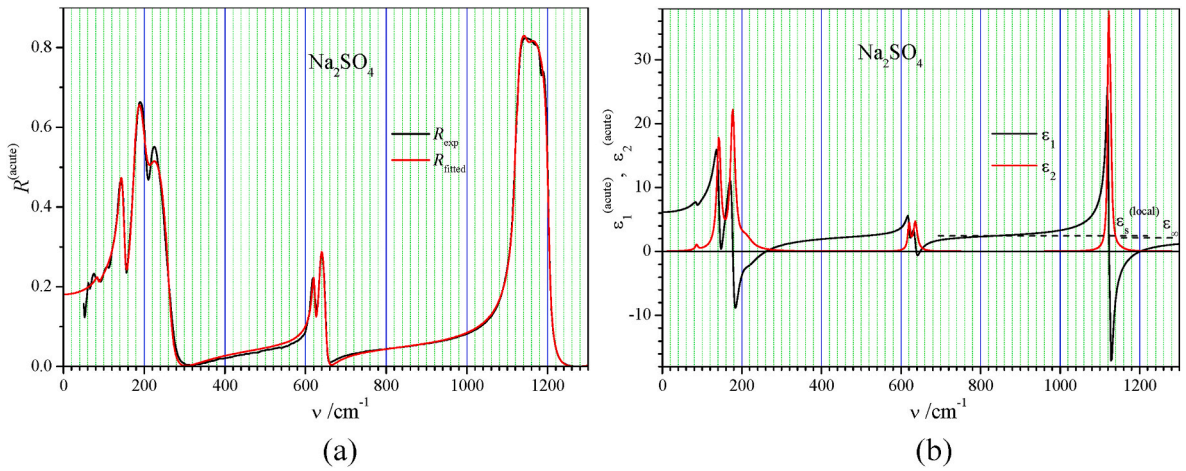

Fig. 9. (a) Experimental (black curve) and fitted (red curve) reflection spectra for radiation polarization along the acute bisector of the angle between optical axes of Na_2SO_4; (b) dielectric function $\varepsilon(\nu) = \varepsilon_1(\nu) + i{\cdot}\varepsilon_2(\nu)$ for the fitted reflection spectrum of Na_2SO_4 (for red curve in Fig. 9(a)). (For interpretation of the references to color in this figure legend, the reader is referred to the Web version of this article.)

Table 8
Fitting parameters of the Drude-Lorentz model (6) corresponding to the radiation polarization along the acute bisector of the angle between optical axes of Na_2SO_4 crystal.

i Parameter	1	2	3	4	5	6	7	8	9
ε_∞	2.1394								
ν_0/cm^{-1}	85.68	142.06	177.18	210.89	620.22	636.08	1121.70	1126.16	1150.03
ν_p/cm^{-1}	22.66	173.16	231.27	120.15	134.62	187.0	409.82	431.12	82.70
γ/cm^{-1}	7.385	12.458	14.176	40.017	7.227	12.084	5.099	7.553	24.257

We have calculated the value of TO-LO splitting corresponding to the Reststrahlen band in the range 1120–1200 cm^{-1} using CASTEP code and have found the value of this splitting, $\Delta\nu^{(LO-TO)} = 70\ cm^{-1}$ (Fig. 10). The obtained value of $\Delta\nu^{(LO-TO)}$ is practically the same as that detected in the reflection experimental spectrum, $\Delta\nu^{(Reststrahlen\ band)} = 1200 - 1120 = 80\ cm^{-1}$ (Fig. 8).

4. Conclusions

The Na_2SO_4 crystal is optically positive, and the $n_Y > n_Z > n_X$ relation holds for its refractive indices in the studied 400–750 nm spectral range at room temperature. The cationic substitution Li → Na leads to an increase in the molar refractivity and polarizability of the crystals.

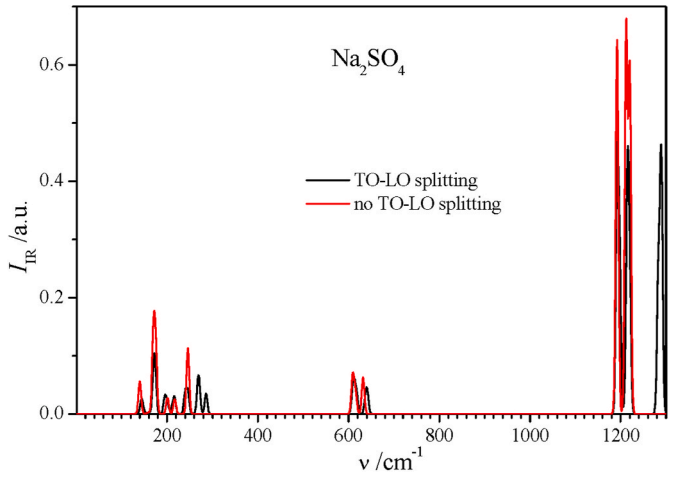

Fig. 10. Infrared spectra of Na_2SO_4 crystal calculated with GGA-PBEsol functional using the norm-conserving pseudopotentials for the cases with (black curve) and without (red curve) TO-LO splitting. (For interpretation of the references to color in this figure legend, the reader is referred to the Web version of this article.)

The experimental polarized reflection spectra of Na_2SO_4 obtained in the far-IR range of 50–1300 cm^{-1} using FTIR spectrometer and synchrotron radiation reveal that (1) the reflection spectral band 1120 - 1200 cm^{-1} relates to the asymmetric stretching vibrations of S - O bonds, (2) the reflection spectral band 610 - 650 cm^{-1} relates to the asymmetric bending vibrations of O - S – O bonds, and (3) the reflection spectral band 100 - 260 cm^{-1} relates to the bonded vibrations of Na^+ cations and SO_4^{2-} anions.

The polarized along the acute bisector of the angle between optical axes of Na_2SO_4 the static dielectric permittivity ε_{0Y} for of Na_2SO_4 crystal is determined to be equal to $\varepsilon_{0Y}^{(exp)} = 6.142$. The calculated value of $\varepsilon_{0Y}^{(calc)} = 6.91158$ obtained using GGA-PBEsol exchange-and-correlation functional and the norm-conserving pseudopotentials is 12 % larger, that is partly caused by the known shortcoming of the local density approximation used. The experimental difference, $\varepsilon_{0Y}^{(exp)} - \varepsilon_{\infty Y}^{(exp)} = 3.9377$, showing the ionic input to the static dielectric permittivity, $\varepsilon_{0y}^{(exp)} = 6.142$, is almost twice larger than the corresponding electronic one, $\varepsilon_{\infty Y}^{(exp)} = 2.2043$. Thus, the structure of Na_2SO_4 crystal may be regarded as relatively high susceptible to the low-frequency electric field.

The high reflection coefficient of Na_2SO_4 crystal ($R \approx 0.8$) in the narrow spectral range 1120–1200 cm^{-1} is caused by the Reststrahlen effect due to the strong TO-LO modes interaction associated with stretching interatomic S - O vibrations.

CRediT authorship contribution statement

M. Ya Rudysh: Writing – review & editing, Writing – original draft, Software, Formal analysis, Data curation. **B.V. Andriyevsky:** Writing – review & editing, Writing – original draft, Supervision, Software, Methodology, Investigation, Formal analysis, Conceptualization. **P.A.**

Shchepanskyi: Visualization, Methodology, Investigation, Formal analysis, Data curation. **M. Karkulovska:** Visualization, Investigation, Formal analysis, Data curation. **V. Yo Stadnyk:** Writing – original draft, Visualization, Validation, Methodology, Investigation, Conceptualization. **L. Bychto:** Visualization, Validation, Methodology, Investigation, Formal analysis, Data curation. **R.S. Brezvin:** Visualization, Validation, Investigation, Formal analysis, Data curation.

Declaration of competing interest

The authors declare the following financial interests/personal relationships which may be considered as potential competing interests: Bohdan Andriyevsky reports a relationship with Koszalin University of Technology that includes: employment. If there are other authors, they declare that they have no known competing financial interests or personal relationships that could have appeared to influence the work reported in this paper.

Acknowledgments

Results presented in this work have been obtained with the support of the Project of Young Scientists « New dual-purpose single-, poly- and nanocrystalline materials for batteries, hydrogen accumulators, sensor technology and electronics» (grant number 0123U100599) of the Ministry of Education and Science of Ukraine. This work was partially supported by the Ministry of Education and Science of Ukraine (grant number 0124U001228).

The experimental measurements of infrared spectra of Na_2SO_4 crystal were performed with infrared synchrotron radiation at the IRIS beamline of the electron storage ring BESSY II at the Helmholtz-Zentrum Berlin für Materialien und Energie (HZB BESSY project 232-12203-ST). Authors are thankful for U. Schade, L. Puskar, and A. Veber for their support during experiments at the IRIS beamline.

Computer calculations were performed at ICM of Warsaw University, Poland (projects No. g96–1832 and g100-2206) and WCSS of Wrocław University of Technology, Poland (project No. 053).

Data availability

Data will be made available on request.

References

[1] S. Zhu, Y. Sun, K. Li, Y. Dang, X. Guan, Construction of structural supercapacitor with high energy density and mechanical strength based on dual-carbon electrodes and polyacrylamide-Portland cement-Na_2SO_4 electrolyte, J. Power Sources 597 (2024) 234150, https://doi.org/10.1016/j.jpowsour.2024.234150.

[2] W. Huang, G. Zhou, Molecular dynamics simulation of heat, mass and phonon transport performances of nanoparticle enhanced $Na_2SO_4{\cdot}10H_2O$, J. Mol. Liq. 397 (2024) 124157, https://doi.org/10.1016/j.molliq.2024.124157.

[3] F. Omer, Y. Abdulla, A.M. Noh, Preparation and thermoluminescence properties of polycrystalline Na_2SO_4/SiO_2 composite, Braz. J. Radiat. Sci. 12 (2024) 1, https://doi.org/10.15392/2319-0612.2024.2322, 16. e2322-e2322.

[4] S.E. Rasmussen, J.E. Jørgensen, B. Lundtoft, Structures and phase transitions of Na_2SO_4, J. Appl. Crystallogr. 29 (1996) 42–47, https://doi.org/10.1107/S0021889895008818.

[5] B. K Choi, D.J. Lockwood, Peculiarities of the structural phase transitions in Na_2SO_4 (V): a raman scattering study, J. Phys. 17 (2005) 6095, https://doi.org/10.1088/0953-8984/17/38/013.

[6] V. Correcher, J. Garcia-Guinea, P. Lopez-Arce, J.M. Gomez-Ros, Luminescence emission spectra in the temperature range of the structural phase transitions of Na_2SO_4, Spectrochim. Acta 60 (2004) 1431–1438, https://doi.org/10.1016/j.saa.2003.08.008.

[7] V. Yu Proydakova, V.V. Voronov, A.A. Pynenkov, S.V. Kuznetsov, M.P. Zykova, K. N. Nishchev, P.P. Fedorov, Sodium sulfate polymorphism, Russ. J. Inorg. Chem. 67 (2022) 970–977, https://doi.org/10.1134/S0036023622070208.

[8] P. D. Sahare Pandey, Thermoluminescence characteristics of $LiNaSO_4$ doped with rare earths Eu and Dy, Phys. Stat. Sol. A 199 (2003) 533–540, https://doi.org/10.1002/pssa.200306655.

[9] R.A. Secco, E.A. Secco, Effect of pressure on the electrical conductivity, na^+-Ion transport, in Na2SO4, J, Phys. Chem. Solids 53 (1992) 749–753, https://doi.org/10.1016/0022-3697(92)90184-F.

[10] B.-K. Choi, D.J. Lockwood, Ionic conductivity and the phase transitions in Na_2SO_4, Phys. Rev. B 40 (7) (1989) 4683–4689, https://doi.org/10.1103/PhysRevB.40.4683.

[11] B.-K. Choi, Ionic conductivity of Na_2SO_4 (I) crystals, Solid State Ionics 58 (1992) 133–138, https://doi.org/10.1016/0167-2738(92)90020-P.

[12] C. Li, B. Zhang, B. Xie, X. Zhao, J. Chen, Tailored phase change behavior of $Na_2SO_4{\cdot}10H_2O$/expanded graphite composite for thermal energy storage, Energ Convers Manage 208 (2020) 112586, https://doi.org/10.1016/j.enconman.2020.112586.

[13] STOE & Cie GmbH, Winxpow 3.03, Powder Diffraction Software Package, 2010. Darmstadt, Germany.

[14] W. Kraus, G. Nolze, Powder cell - a program for the representation and manipulation of crystal structures and calculation of the resulting X-ray powder patterns, J. Appl. Cryst. 29 (1996) 301–303.

[15] M.O. Romaniuk, Crystal Optics, Ivan Franko LNU, Lviv, 2017.

[16] G. Boyd, H. Kasper, J. McFee, F. Storz, Linear and nonlinear optical properties of some ternary selenides, IEEE J. Quantum Electron. 8 (1972) 900–908, https://doi.org/10.1109/JQE.1972.1076900.

[17] M.O. Romaniuk, Workshop on Crystal Optics and Crystal Physics, Ivan Franko LNU, Lviv, 2012.

[18] B. Andriyevsky, L. Bychto, K. Dorywalski, U. Schade, L. Puskar, A. Patryn, A. Hapka, K. Mydłowska, A. Veber, A.I. Kashuba, K.T.R. Reddy, The optical properties of In_2S_3 films in the far-infrared spectral range, Infrared Phys Techn 131 (2023) 104662, https://doi.org/10.1016/j.infrared.2023.104662.

[19] S.J. Clark, M.D. Segall, C.J. Pickard, P.J. Hasnip, M.I.J. Probert, K. Refson, M. C. Payne, First principles methods using CASTEP, zeitschrift FÄĽr kristallographie -, Crystalline Materials 220 (2005) 567–570, https://doi.org/10.1524/zkri.220.5.567.65075.

[20] S. Baroni, S. de Gironcoli, A. Dal Corso, P. Giannozzi, Phonons and related crystal properties from density-functional perturbation theory, Rev. Mod. Phys. 73 (2001) 515–562, https://doi.org/10.1103/RevModPhys.73.515.

[21] K. Refson, P.R. Tulip, S.J. Clark, Variational density-functional perturbation theory for dielectrics and lattice dynamics, Phys. Rev. B 73 (2006) 155114, https://doi.org/10.1103/PhysRevB.73.155114.

[22] A.I. Kashuba, M.V. Solovyov, T.S. Maliy, I.A. Franiv, O.O. Gomonnai, O. V. Bovgyra, O.V. Futey, A.V. Franiv, V.B. Stakhura, Lattice vibration spectra of A_4BX_6 group crystals, J. Phys. Stud. 22 (2018) 2701, https://doi.org/10.30970/jps.22.2701.

[23] J.P. Perdew, K. Burke, M. Ernzerhof, Generalized gradient approximation made simple, Phys. Rev. Lett. 77 (1996) 3865–3868, https://doi.org/10.1103/PhysRevLett.77.3865.

[24] J.G. Lee, Computational Materials Science: an Introduction, *CRC Press*, Taylor Francis Group, 2012.

[25] J.P. Perdew, J.A. Chevary, S.H. Vosko, K.A. Jackson, M.R. Pederson, D.J. Singh, C. Fiolhais, Atoms, molecules, solids, and surfaces: applications of the generalized gradient approximation for exchange and correlation, Phys. Rev. B 46 (1992) 6671–6687, https://doi.org/10.1103/PhysRevB.46.6671.

[26] D.R. Hamann, M. Schluter, C. Chiang, Norm-conserving pseudopotentials, Phys. Rev. Lett. 43 (1979) 1494–1497.

[27] B.G. Pfrommer, M. Côté, S.G. Louie, M.L. Cohen, Relaxation of crystals with the quasi-newton method, J. Comput. Phys. 131 (1997) 233–240, https://doi.org/10.1006/jcph.1996.5612.

[28] M.Y. Rudysh, M.G. Brik, O.Y. Khyzhun, A.O. Fedorchuk, I.V. Kityk, P. A. Shchepanskyi, V.Y. Stadnyk, G. Lakshminarayana, R.S. Brezvin, Z. Bak, M. Piasecki, Ionicity and birefringence of α-$LiNH_4SO_4$ crystals: ab initio DFT study, X-ray spectroscopy measurements, RSC Adv. 7 (2017) 6889–6901, https://doi.org/10.1039/C6RA27386F.

[29] W.H. Zachariasen, G.E. Ziegler, The crystal structure of anhydrous sodium sulfate Na_2SO_4, Cristallographic, Kristallgeometric, Kristallphysik, Kristallchemie 81 (1932) 92–101.

[30] K. Momma, F. Izumi, VESTA 3 for three-dimensional visualization of crystal, volumetric and morphology data, J. Appl. Crystallogr. 44 (2011) 1272–1276, https://doi.org/10.1107/S0021889811038970.

[31] P.A. Shchepanskyi, V.Yo Stadnyk, M.Ya Rudysh, R.S. Brezvin, B.V. Andrievskii, Energy band structure and optical properties of $LiNaSO_4$ crystals, Opt. Spectrosc. 125 (2018) 353–357, https://doi.org/10.1134/S0030400X18090217.

[32] M.Ya Rudysh, P.A. Shchepanskyi, O.Y. Khyzhun, A.K. Sinelnichenko, R.S. Brezvin, V.Yo Stadnyk, A.O. Fedorchuk, Structure, optical, and electronic properties of sodium ammonium sulfate dehydrate crystal, Opt. Mater. 158 (2025) 116501, https://doi.org/10.1016/j.optmat.2024.116501.

[33] V. Yo Stadnyk, M.O. Romanyuk, O.Z. Chyzh, V.F. Vachulovych, The baric changes of the refractive properties of K_2SO_4 crystals, Condens. Matter Phys. 10 (2007) 45–50, https://doi.org/10.5488/CMP.10.1.45.

[34] P.A. Shchepanskyi, O.S. Kushnir, V. Yo Stadnyk, R.S. Brezvin, A.O. Fedorchuk, Structure and refractive properties of $LiNaSO_4$ single crystals, Ukr. J. Phys. Optics 19 (2018) 141–149.

[35] Z. Bo, S. Qing, H. De-Yan, First-principles calculations on the electronic and vibrational properties of β-V_2O_5, Chinese Phys. B 18 (2009) 4988–4994, https://doi.org/10.1088/1674-1056/18/11/062.

[36] P.J. Stephens, F.J. Devlin, C.F. Chabalowski, M.J. Frisch, Ab initio calculation of vibrational absorption and circular dichroism spectra using density functional force fields, J. Phys. Chem. 98 (1994) 11623–11627, https://doi.org/10.1021/j100096a001.

[37] M.Ya Rudysh, A.I. Kashuba, V.Yo Stadnyk, R.S. Brezvin, P.A. Shchepanskyi, V. M. Gaba, Z.O. Kohut, Raman scattering spectra of β-$LiNH_4SO_4$ crystals, J. Appl. Spectrosc. 85 (2019) 1022–1028, https://doi.org/10.1007/s10812-019-00754-z.

[38] M. Ya Rudysh, P.A. Shchepanskyi, G.L. Myronchuk, M. Piasecki, O.S. Martyniuk, Vibrational, thermodynamic and acoustic properties of $AgAlS_2$ crystal, Phys. B Condens. Matter 654 (2023) 414731, https://doi.org/10.1016/j.physb.2023.414731.
[39] M. Ya Rudysh, M. Piasecki, G.L. Myronchuk, P.A. Shchepanskyi, V. Yo Stadnyk, O. R. Onufriv, M.G. Brik, $AgGaTe_2$ - the thermoelectric and solar cell material: structure, electronic, optical, elastic and vibrational features, Infrared Phys. Techn. 111 (2020) 103476, https://doi.org/10.1016/j.infrared.2020.103476.
[40] O.V. Bovgyra, V. Yo Stadnyk, O.Z. Chyzh, Energy band structure and refractive properties of $LiRbSO_4$ crystals, Phys. Solid State 48 (7) (2006) 1268–1272.
[41] C. Kittel, Introduction to Solid State Physics, eighth ed., Wiley, 2005.
[42] K. Nakamoto, Infrared and Raman Spectra of Inorganic and Coordination Compounds, fifth ed., Wiley, New York, 1997.
[43] X. Gonze, C. Lee, Dynamical matrices, born effective charges, dielectric permittivity tensors, and interatomic force constants from density-functional perturbation theory, Phys. Rev. B 55 (1997) 10355–10368.
[44] V. Stadnyk, B. Andriyevsky, I. Pryshko, L. Bychto, Z. Kohut, U. Schade, A. Veber, L. Puskar, R. Brezvin, Piezo-optical properties and infrared spectra of Rb_2SO_4 crystals, Opt. Mater. 157 (2024) 116320.
[45] A.B. Kuzmenko, Kramers-kronig constrained variational analysis of optical data, Rev. Sci. Instrum. 76 (2005) 083108.
[46] P.Y. Yu, M. Cardona, Fundamentals of Semiconductors, Springer Heidelberg, Dordrecht London New York, 2010.
[47] S. Foteinopoulou, G.C.R. Devarapu, G.S. Subramania, S. Krishna, D. Wasserman, Nanophotonics 8 (2019) 2129–2175.
[48] F.E. Volz, Infrared specular reflectance of pressed crystal powders and mixtures, Appl. Opt. 22 (1983) 1842–1855.
[49] W.D. Callister JR., D.G. Rethwisch, Materials Science and Engineering. an Introduction, ninth ed., John Wiley & Sons, Inc., New Jork, 2000. Copyright © 2014, 2010, 2007, 2003.